LONDON, METEOROLOGICAL OFFICE.

Met.O.19 Branch Memorandum No.58.

Direct use of Meteosat water vapour channel radiances to improve the humidity analysis in a forecast model. By EYRE,J.R.

London,Met.Off.,Met.O.19 Branch Mem.No.58, 1980,31cm.Pp.5,10 pls.+App.6.8 Refs.

An unofficial document - restriction on first page to be observed.

MET O 19 BRANCH MEMORANDUM NO 58

DIRECT USE OF METEOSAT WATER VAPOUR CHANNEL RADIANCES TO IMPROVE THE HUMIDITY ANALYSIS IN A FORECAST MODEL

by

EYRE J R

Met O 19
(Satellite Meteorology Branch),
Meteorological Office
London Road
Bracknell
Berkshire
RG12 2SZ

July 1980

DIRECT USE OF METEOSAT WATER VAPOUR CHANNEL RADIANCES TO IMPROVE THE HUMIDITY ANALYSIS IN A FORECAST MODEL

1. Introduction

The Meteosat channel at 6.5μm (the WV channel) senses radiation emitted by water vapour in the middle and upper troposphere and, if present, by clouds in these layers. For a clear atmosphere of average absolute humidity, the level contributing the most radiation lies between 400 and 450 mb (Roulleau et al, 1980), although this level moves up to about 350 mb and down to about 550 mb for extreme examples of wet and dry atmospheres respectively. Even for the drier atmospheres there is negligible contribution to the radiance from below 700 mb. In the presence of cloud, the WV channel senses radiation emitted partly from the cloud top and partly from the water vapour in the clear air above the cloud.

If the temperature profile is known, the measured WV channel radiance can be used to estimate the humidity at the levels from which the radiation originates. From one radiance it is not possible to retrieve a humidity profile, but if the shape of the profile is assumed (from climatology or a forecast model) either the mean relative humidity in these layers or the total water vapour content above a given level (say, 500 mb for this channel) can be estimated.

It is ESOC's intention (Meteosat System Guide, 1980) to analyse Meteosat WV channel imagery in real time to obtain an "upper tropospheric humidity product" in the form of average relative humidities for the upper troposphere with a resolution ~ 140 km x 140 km at the sub-satellite point (0°N 0°E) degrading to ~ 300 km x 150 km at 50°N 0°E. This product should be available when Meteosat 2 becomes operational and could then be added to conventional observations to improve the humidity analysis of numerical forecast models. At present retrievals are only planned within a 50° great circle arc of the sub-satellite point. This area includes only about one third of the Meteorological Office operational 10-level model "rectangle" area (see figure 1). The proposed product also has other drawbacks. In areas of complete cover of high or medium level cloud no retrieval is attempted. In areas of partial cover of such cloud, the product is biased towards the clear air values. Also, the retrieval scheme is forced to use forecast temperature fields (from the US National Weather Service, though possibly from ECMWF in future). Analysed temperature fields would be more appropriate.

The scheme described here uses a more direct approach to improve the humidity analysis at the upper levels of the 10-level model. The temperature and humidity analyses of the "rectangle" model are combined with a radiative transfer scheme to calculate the expected WV channel radiance for each model grid point. The Meteosat WV image is projected on to the "rectangle" grid and the difference between the measured and simulated radiances is used to correct the humidity profile so that the simulated radiance corresponding to the new profile is in better agreement with the measured radiance. By excluding only those parts of the image for which the zenith angle at the earth's surface is greater than 80°, the scheme can be applied to 87% of the "rectangle" - all but the NW corner.

The results show that the information contained in the WV image allows considerable improvement of the humidity analysis. The impact on forecasts from the increased accuracy of upper level humidities would probably be small at present. However, forecasting requirements and techniques which could benefit from such an improved analysis may develop in the future. Also the method used illustrates how satellite-measured radiances can be included directly in an analysis and it may be possible to extend the technique to other satellite data.

2. Method

a. Re-projection of the image

A Meteosat WV image taken close to a synoptic hour is processed to give average values over 4 x 4 pixel squares. (A pixel or picture element is the basic unit from which the image is constructed. A WV image of the full earth's disc is 2500 x 2500 pixels and each represents an average brightness value over an area ~5 km x 5 km. Each pixel is transmitted in digital form from the satellite and must be converted into radiance units, if required, using calibration data.) The averaging process reduces the random noise to ~1.5 digital counts (equivalent to ~0.3K for brightness temperatures ~250K) and speeds up the subsequent re-projection process. No resolution is lost as the 4 x 4 squares are still smaller than the "rectangle" grid spacing. The position of each 4 x 4 square is converted to latitude-longitude co-ordinates and is then re-projected to "rectangle" grid co-ordinates (polar stereographic). The square is assigned to the nearest "rectangle" grid point. The mean WV value in digital counts at each grid point is calculated by taking the mean of all the 4 x 4 squares assigned to it. In the SE corner of the "rectangle", ~15 squares are assigned to each grid point. This number falls to 1 or 2 squares at the NW limit of the usable data (see figures 1 and 2).

b. Initial temperature and humidity fields

The analysed fields of temperature and humidity for the "rectangle" at the synoptic hour are obtained. (This experiment used archived data in which temperature and relative humidity are stored at standard pressure levels). From these values profiles are interpolated at 50 mb intervals from 1000 mb to 50 mb. This vertical grid has been found adequately small for accurate integration of the radiative transfer equation (Eyre, 1979). Humidity values are not available above 400 mb; the model itself does not represent humidity above 350 mb. Therefore humidity is extrapolated above 400 mb by assuming a constant relative humidity in the troposphere and a constant mass mixing ratio of 3×10^{-6} at 150 mb and above (ie a typical stratospheric value).

c. Calculation of radiance

The temperature and humidity profile at each grid point are used as input to a radiative transfer scheme developed for the 6.5 μm water vapour band (see appendix A) to simulate the radiance at the satellite. This calculation involves assumptions about the cloud amounts at each level. All clouds are assumed to have an emissivity of 1 and to have a fractional cover given by:

$$\text{fractional cover} = \begin{cases} 1 & \text{for RH} > 0.9, \\ (\text{RH}/0.45) - 1 & \text{for } 0.45 \leq \text{RH} \leq 0.9, \\ 0 & \text{for RH} < 0.45, \end{cases} \qquad 2.1$$

where RH is the relative humidity at that level. This is the empirical algorithm used in the 10-level model for medium level cloud (Burridge and Gadd, 1977). The horizontal positions of clouds at different levels are assumed to be highly correlated. For example, if there are clouds at 2 levels, a fraction x at level 1 and a fraction y at a lower level 2, then the fractional cover "seen" by the satellite is:

at level 1, x,
at level 2, $(y-x)$ for $y \geq x$, with $(1-y)$ clear,
and 0 for $y < x$, with $(1-x)$ clear.

However it has been shown by experiment that the simulated radiance is not very sensitive to the degree of correlation assumed.

No attempt is made to simulate cloud above 400 mb. In areas of extensive high cloud this leads to overestimation of the simulated radiance. This must be borne in mind when interpreting the results of this experiment, but it does not appear to be a major problem and could be improved by a more sophisticated treatment of the extrapolation of humidity and cloud above 400 mb.

d. Adjustment of the humidity field

The measured mean WV value in digital counts at each grid point is first calibrated to give a radiance. This can be done by the best available method. In this experiment a calibration constant of 5.188×10^{-5} $Wm^{-2}sr^{-1}(cm^{-1})^{-1}$ $count^{-1}$ was used - appropriate to Meteosat WV images for 29 November 1978 and obtained using aircraft data (Eyre, 1979). The measured and simulated radiances are converted to brightness temperatures, T_m and T_c respectively. The relative humidity at each level from 700 mb to 200 mb is then adjusted using the expression,

$$RH_{new} = RH_{old} \exp\left(A(T_m - T_c)W\right) \qquad 2.2$$

The form of this correction is justified in appendix B, where it is shown that a value of A appropriate to clear air calculations can be calculated for each individual profile. However, a statistical treatment has been used here to find average values of A to be applied to all profiles. This method implicitly includes the effects of clouds as well as clear air. The initial profiles are used to calculate brightness temperatures. The profiles are then adjusted - any realistic adjustment will suffice - and the new profiles used to calculate new brightness temperatures. Using an equation of the form of 2.2 with W = 1, RH_{new} and RH_{old} at 400 mb and $(T_c)_{new}$ and $(T_c)_{old}$ provide a statistical base for the calculation of values of A. The values obtained by this method and used in this experiment were

$$A = -0.125 \text{ for } T_m \geqslant T_c$$
$$\text{and } A = -0.093 \text{ for } T_m < T_c.$$

The factor W is included to prevent the adjustment of relative humidities at levels below those from which most of the radiation originates. T_m is converted to a pressure level, p_m, by interpolation on the temperature profile. Then, at pressure level, p,

$$\left.\begin{aligned} W &= 1 \quad \text{for } p \leqslant p_m \\ \text{and } W &= \exp\left\{-(p-p_m)^2/\Delta p^2\right\} \text{ for } p > p_m. \end{aligned}\right\} \qquad 2.3$$

Δp was chosen empirically as 200 mb based on the shape of the contribution functions given by Roulleau et al (1980). RH_{new} was not allowed to be higher than 100% and, in this experiment, no changes were allowed for levels below 700 mb and above 200 mb.

The new values of relative humidity represent the humidity field adjusted to take account of the measured radiances. The degree of compatibility between the measured radiances and the new field can be assessed by repeating step (c) with the new profile and comparing the new simulated radiances with the measurements.

3. Results

The experiment was performed using archived "rectangle" data for 29 November 1978 at 1200Z. The Meteosat WV image used was slot 26 for this day (taken between 1230Z and 1300Z). The initial humidity fields at 400 and 500 mb are given in figures 7(a) and 7(b) respectively, which show relative humidities as percentages. Figures 2 and 3 show respectively the calibrated measured radiances and the radiances simulated from the initial field both in units of $mWm^{-2}sr^{-1}(cm^{-1})^{-1}$, and figure 4 gives their absolute difference in $mWm^{-2}sr^{-1}(cm^{-1})^{-1}$ x 10. The humidity fields after adjustment are given in figures 8(a) and 8(b) and the corresponding simulated radiances in figure 5. The remaining difference between the measurements and the new simulated radiances is shown in figure 6.

Comparison of figures 2 and 3 shows that there is considerably more structure in the measured field. This is understandable since the model analysis of humidity at these levels is probably influenced very strongly by the background field and so tends to become rather smooth. The adjustment process introduces more structure: compare figures 7(a) and (b) with figures 8(a) and (b) or figure 3 with 5. Comparison of figures 2 and 5 shows that the adjustment brings the measured and simulated fields into much better agreement. A notable exception is the area of low radiance towards the SW of the "rectangle". Here the absence of simulated cloud above 400 mb makes it impossible for the simulated radiance to be brought as low as the measured radiance, but the present deficiencies of the scheme in this respect are well understood. Elsewhere agreement is good. Comparison of figure 4 with 6 illustrates the improvement - the area over which the difference is less than 0.5 $mWm^{-2}sr^{-1}(cm^{-1})^{-1}$ (equivalent to ~2K at 250K) is considerably increased.

The mean radiance level for the measured field is ~8% higher than that of the field simulated from the initial analysis. This could be caused either by a calibration error or a bias in the analysed humidities at upper levels in the model.

Most of the computer time used in this process is in steps (a) and (c) which currently take 19s and 53s of CPU time respectively on the IBM 360/195. However, no special effort has been made to optimize either programme and improvements by factors ~3 are thought possible.

4. Possible improvements

a. The extrapolation of humidity profiles above 400 mb could be improved to take account of the temperature profile and the climatology of humidity profiles. Also, cloud layers compatible with the humidity extrapolation could be included above 400 mb.

b. The method described in section 2 requires just one simulation of radiance; the second is only for comparison purposes. However the results of the second simulation could be used in conjunction with the measured radiances, the first simulation and the old and new humidity fields to make a fine adjustment to the new humidity field to correct for the remaining difference between the measured and calculated radiances.

c. The simulation of cloud could be more sophisticated.

d. The equation used to correct the humidity profile could be studied to assess the most appropriate values of the factor, A, and the form of the variable, W. The value of Δp in equation 2.3 and the most appropriate form of this equation, particularly in the presence of cloud, are both open to question. The aim should be to make no unwarranted humidity adjustments at lower levels.

e. The Meteosat 11μm (IR) channel could also be projected on to the "rectangle" grid to improve the treatment of cloud.

5. Comments

The results shown here are encouraging and demonstrate that considerable improvements in the humidity analysis are possible, even with only one calculation of the simulated radiance field. With more simulations further adjustments are possible by successive approximation. Also, the corrections in this experiment are rather large, as the analysis had no "previous knowledge" of this type of data. In an operational scheme updating perhaps once or twice a day the corrections to the initial field would probably be smaller.

The accuracy of the humidities obtained by this method is dependent on the accuracy of the analysed temperature field. A 1K error in temperature will lead to ~10% error in mixing ratio. However this is relatively unimportant in the present experiment since more than half of the adjustments to the mixing ratios (ie the absolute humidities) are >50%.

This method uses radiances directly and bypasses the intermediate product of humidities used by conventional analysis schemes. This approach may have advantages over those currently used for satellite data. Given direct access to real-time satellite data it would certainly speed up the availability of the product. Also, it may be possible to extend such a technique to other forms of satellite data - perhaps the temperature and humidity sounding channels on the TIROS-N series. (A TIROS-N pass covers up to one third of the "rectangle" area, though it may not coincide with a synoptic hour).

The method presented here is quite flexible and could be incorporated into an analysis scheme in several ways. It could follow the conventional analysis just as described here, or it could be applied to the background humidity field before the conventional observations are incorporated (though preferably after the temperature field has been updated). Alternatively, rather than apply the conventional and the "new" forms of analysis successively, they could be integrated; radiosonde observations and satellite data, with appropriate weights, could be combined at the analysis of each individual grid point.

Appendix A - A radiative transfer scheme for the Meteosat WV channel

The radiance reaching the satellite from a column of atmosphere is given by

$$R = \frac{\int_{\nu_1}^{\nu_2} f(\nu)\left\{B(\nu, T_s)\,\tau_\nu(\theta, p_s, 0) + \int_{\tau_\nu(\theta,p_s,0)}^{1} B(\nu, T(p))\, d\tau(\theta, p, 0)\right\} d\nu}{\int_{\nu_1}^{\nu_2} f(\nu)\, d\nu} \qquad \text{A.1}$$

where $f(\nu)$ is the relative spectral response of the radiometer which is sensitive over the range, ν_1 to ν_2,
and T_s is the brightness temperature of the underlying surface (earth's surface or cloud top) at pressure level, p_s,
and $\tau_\nu(\theta, p, 0)$ is the atmospheric transmittance at wavenumber, ν, and zenith angle, θ, between pressure level, p, and space.
The denominator normalises the radiance into units of the Planck function, $B(\nu, T)$: eg $Wm^{-2}sr^{-1}(cm^{-1})^{-1}$.

Equation A.1 is evaluated numerically by performing the atmospheric integration over discrete pressure intervals ($\Delta p = 50$ mb) and the frequency integration over discrete wavenumber intervals ($\Delta\nu = 50\ cm^{-1}$).

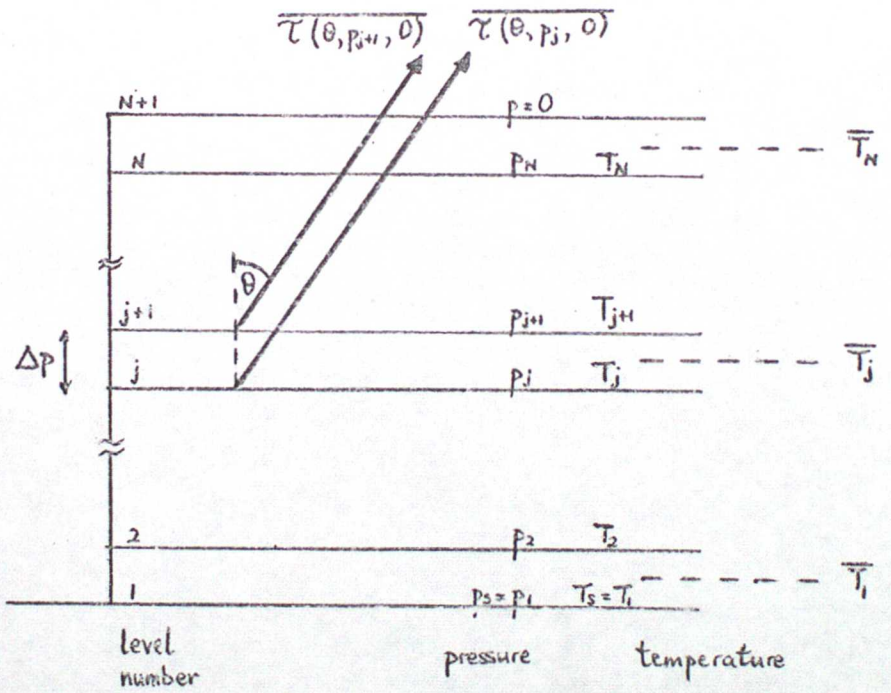

Then,

$$R = \frac{\sum_i F(\nu_i)\left\{B(\nu_i, T_s)\,\overline{\tau_{\nu_i}(\theta, p_s, 0)} + \sum_{j=1}^{N} B(\nu_i, \overline{T}_j)\left[\overline{\tau_{\nu_i}(\theta, p_{j+1}, 0)} - \overline{\tau_{\nu_i}(\theta, p_j, 0)}\right]\right\}}{\sum_i F(\nu_i)}, \qquad \text{A.2}$$

where $F(\nu_i) = \int_{\nu_i - 25\,cm^{-1}}^{\nu_i + 25\,cm^{-1}} f(\nu)\, d\nu$,

and $\overline{\tau_{\nu_i}(\theta, p, 0)} = \frac{1}{50}\int_{\nu_i - 25\,cm^{-1}}^{\nu_i + 25\,cm^{-1}} \tau_\nu(\theta, p, 0)\, d\nu$.

Level $j = 1$ is the surface or cloud top.

$F(\nu_i)$ are precomputed from the WV channel spectral response data (Morgan, 1979) with 11 values of ν_i at 1325, 1375, ..., 1825 cm^{-1}. $\overline{\tau_{\nu_i}(\theta, p, 0)}$ are calculated for each spectral interval of width, $\Delta\nu$, using a Malkmus random band model, which assumes that the spectral lines are randomly positioned within the interval and that the number of lines of strength, S to S + dS, is given by

$$N(S)\,dS = \frac{N_0}{k} \exp\left(-\frac{S}{k}\right) dS . \qquad \text{A.3}$$

N_0 and k are adjusted to fit known spectral line data using the method given by Rodgers (1976) where fitting is performed to give exact agreement in strong and weak absorption limits. The resulting mean transmittance over the interval of width, $\Delta\nu$, is given by

$$\tau(\theta, p, 0) = \exp\left\{-\frac{s^2}{2w}\left[\left(1 + \frac{4w^2}{s^2}\right)^{1/2} - 1\right]\right\}, \qquad \text{A.4}$$

where $$w = \frac{1}{\Delta\nu}\, m(\theta, p, 0) \sum_n S_n$$

and $$s = \frac{2}{\Delta\nu} \sqrt{m(\theta, p, 0)} \sum_n \sqrt{S_n \alpha_n}$$

Here S_n and α_n are the strength and Lorentz half-width of the nth line in the interval and the summations are over all lines in the interval. The values of $\sum_n S_n$ and $\sum_n \sqrt{S_n \alpha_n}$ can be computed from tabulated line data. The values used here for the 6.5μm water vapour band are those given by Houghton (1977) which have been computed from the spectral line data given by McClatchey et al (1973). Houghton's tabulation is at 220K, 260K and 300K. Values at intermediate temperatures can be interpolated using a quadratic temperature dependence to fit the data.

The absorber amount, $m(\theta, p, 0)$, between pressure level, p, and space at zenith angle, θ, is calculated as follows:

$$m(\theta, p, 0) = \int_z^\infty \sec\theta\; c(z)\, \rho(z)\, dz = \sec\theta \int_0^p c(p)\, \frac{dp}{g}, \qquad \text{A.5}$$

where c is the humidity mass mixing ratio and ρ is the density, and the hydrostatic equation, $dp = -g\rho\, dz$, has been applied. The mean temperature and pressure of each path required for the calculation of $\sum_n S_n$ (a function of T) and $\sum_n \sqrt{S_n \alpha_n}$ (a function of p and T) are

$$\overline{p} = \frac{\int p\, dm}{m} \quad \text{and} \quad \overline{T} = \frac{\int T\, dm}{m} \qquad \text{A.6}$$

The integrals in A.5 and A.6 are evaluated in practice by assuming a linear variation of c(p) and T(p) between the pressure levels at 50 mb intervals at which c and T are specified.

The earth's surface is assumed to be black, to be at 1000 mb and to have a temperature equal to the atmospheric temperature at 1000 mb. These approximations are unimportant as the radiation reaching the satellite from the surface is negligible at these wavelengths. Cloud tops simulated at the pressure levels are treated similarly. If the fraction of surface or cloud top at the ℓth level visible from space is x_ℓ and gives rise to a satellite-measured radiance, R_ℓ, then the cloud-contaminated radiance is given by

$$R_{cc} = \sum_{l=1}^{N} R_l x_l \qquad \text{A.7}$$

each R_l being evaluated using A.2.

Appendix B - The relationship between brightness temperature and humidity

The measured brightness temperature is a mean atmospheric temperature weighted according to the amount of radiation originating from each layer of the atmosphere. The brightness temperature, T_{br}, is therefore equal to an atmospheric temperature, $T(p_o)$, at a pressure level, p_o, near the peak of the contribution function:

$$T_{br} = T(p_o) \qquad \text{B.1}$$

As the humidity changes (with constant temperature profile), the level, p_o, rises or falls such that the mean transmittance from p_o to space, $\overline{\tau(\theta, p_o, o)}$, remains approximately constant.

Let us assume that $\overline{\tau(\theta, p_o, o)}$ is only a function of the absorber amount in the path, $m(\theta, p_o, o)$:

$$\overline{\tau(\theta, p_o, o)} = f\{m(\theta, p_o, o)\} \qquad \text{B.2}$$

This assumption is discussed further below.

Also, let us assume a mixing ratio profile,

$$c(p) = b\,p^n \qquad \text{B.3}$$

where for any given profile b and n can be taken as constants over the height range of the contribution function. Then,

$$m(\theta, p_o, o) = \int_{p_o}^{o} -\sec\theta\, c(p)\frac{dp}{g} = \sec\theta\,\frac{b}{g}\int_{o}^{p_o} p^n\,dp = \frac{\sec\theta}{g}\,\frac{b\,p_o^{n+1}}{n+1}. \qquad \text{B.4}$$

To find the change in brightness temperature with changing humidity, we find the dependence of p_o on b at constant m (ie at constant $\overline{\tau}$):

$$\left(\frac{\partial p_o}{\partial b}\right)_m = -\left(\frac{\partial m}{\partial b}\right)_{p_o} \Big/ \left(\frac{\partial m}{\partial p_o}\right)_b \qquad \text{B.5}$$

From B.4,

$$\left(\frac{\partial p_o}{\partial b}\right)_m = -\left\{\frac{\sec\theta}{g}\,\frac{p_o^{n+1}}{n+1}\right\} \Big/ \left\{\frac{\sec\theta}{g}\,b\,p_o^{n}\right\} = \frac{-p_o}{b(n+1)} \qquad \text{B.6}$$

Also, using B.1,

$$\left(\frac{\partial T_{br}}{\partial b}\right)_m = \left(\frac{\partial T(p_o)}{\partial b}\right)_m = \frac{dT(p_o)}{dz}\cdot\frac{dz}{dp_o}\left(\frac{\partial p_o}{\partial b}\right)_m \qquad \text{B.7}$$

Substituting into B.7 from B.6, the hydrostatic equation and the gas law,

$$\left(\frac{dT_{br}}{db}\right)_m = \frac{dT(p_o)}{dz}\left\{\frac{RT(p_o)}{-gp_o}\right\}\left\{\frac{-p_o}{b(n+1)}\right\} .$$

$$\therefore \frac{db}{b} = A\, dT_{br}, \quad \text{where} \quad A = \left\{\frac{dT(p_o)}{dz}\,\frac{RT(p_o)}{g(n+1)}\right\}^{-1} . \qquad \text{B.8}$$

If we take A as constant, then by integration,

$$b_2 = b_1 \exp\{A(T_2 - T_1)\}, \qquad \text{B.9}$$

where $T_{br} = T_1$ when $b = b_1$, and $T_{br} = T_2$ when $b = b_2$.

The change in mixing ratio or relative humidity can be expressed in the same way as B.9.

A will not be constant from profile to profile as it depends on $T(p_o)$, $dT(p_o)/dz$ and n. It can therefore be calculated for each profile individually or else an average value can be found statistically from the dependence of ΔT_{br} on Δb as calculated by radiance simulations. The latter method has been used in this experiment.

The original assumption that $\overline{\tau(\theta, p_o, 0)}$ is a function of $m(\theta, p_o, 0)$ only is questionable. A better approximation for a strong absorption band is that $\overline{\tau(\theta, p_o, 0)}$ is a function of the variable, $p_o^{\epsilon}\, m(\theta, p_o, 0)$, where $0 < \epsilon < 1$. This gives rise to an expression similar to B.8:

$$\frac{db}{b} = A\, dT_{br}, \quad \text{where} \quad A = \left\{\frac{dT(p_o)}{dz}\,\frac{RT(p_o)}{g(\epsilon+n+1)}\right\}^{-1} . \qquad \text{B.10}$$

Since n is usually ~ 3, the form of the result is not significantly different from B.8 and the same statistical technique for finding A may be used.

References

Burridge D M, Gadd A J
Meteorological Office Scientific Paper No 34 (1977).
The Meteorological Office operational 10-level numerical weather prediction model (December 1975).

Eyre J R
Met O 19 Branch Memorandum No 53 (1979).
A calibration for the water vapour channel of Meteosat based on aircraft measurements of temperature and humidity.

Houghton J T
Cambridge University Press (1977).
The physics of atmospheres, Appendix 10.

McClatchey R A, Benedict W A, Clough S A, Burch D E, Calfee R F, Fox K, Rothman L S, Garing J S
AFCRL Report TR-73-0096, Env Res Pap 434 (1973).
AFCRL atmospheric absorption line parameters compilation.

* Meteosat System Guide, ESA publication (1980).
(Note: This document is at present in the preliminary stages of publication).

* Morgan J
Meteosat 1, Calibration Report, Issue 3, ESA publication (1979).

Rodgers C D
NCAR Technical Note, NCAR/TN-116 + 1A (March 1976).
Approximate methods of calculating transmission by bands of spectral lines.

* Roulleau M, Poc M M, Scott N A, Chedin A
Proceedings of the 2nd Meteosat Scientific User Meeting (March 1980).
Quantitative studies of Meteosat water vapour data.

* These are ESA publications available from:
ESOC/MDMD, Robert Bosch Strasse 5, 6100 Darmstadt, W Germany.

Figure 1

10-LEVEL MODEL RECTANGLE GRID POINTS

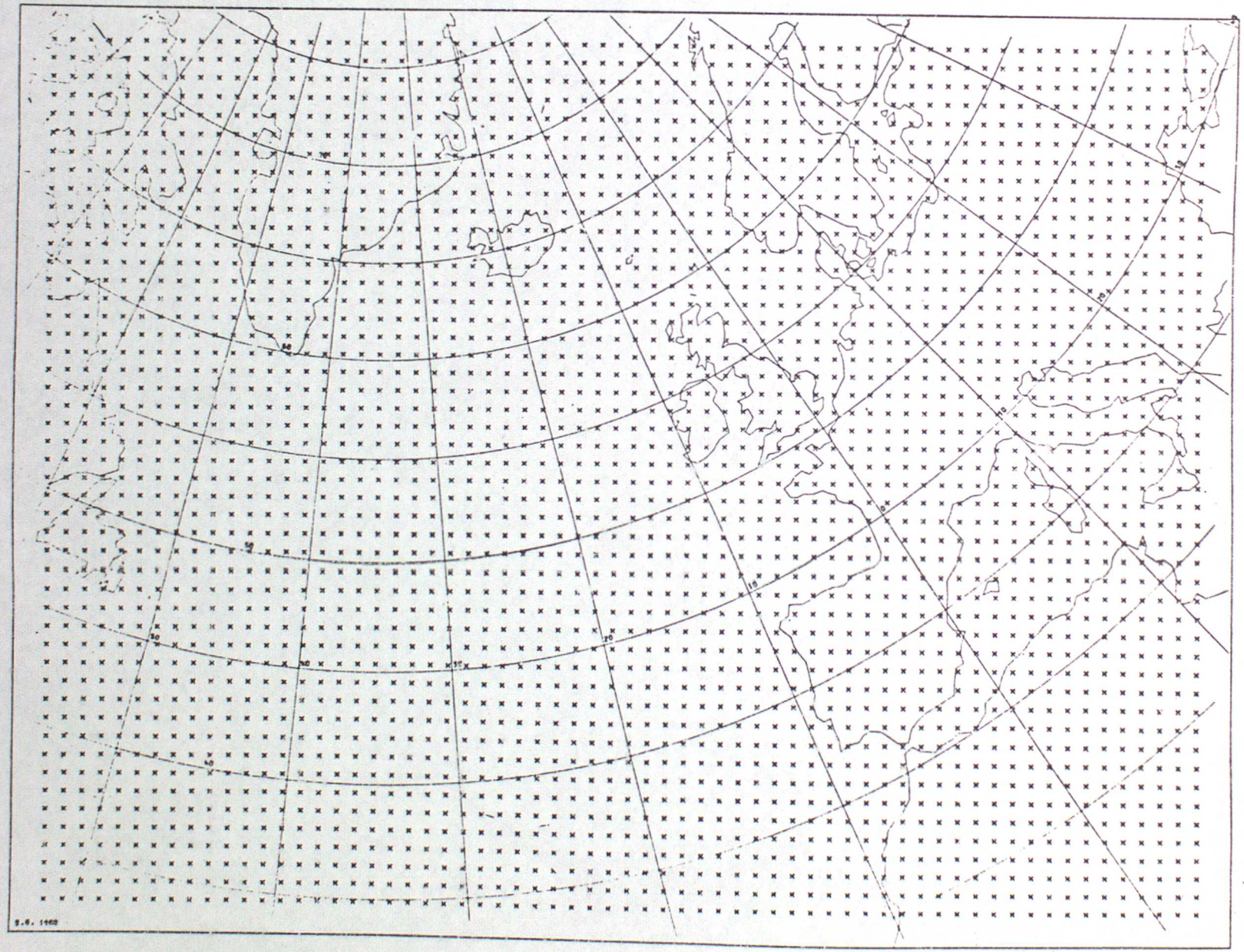

Figure 2 Measured Meteosat WV channel image : calibrated and projected on to "rectangle" grid

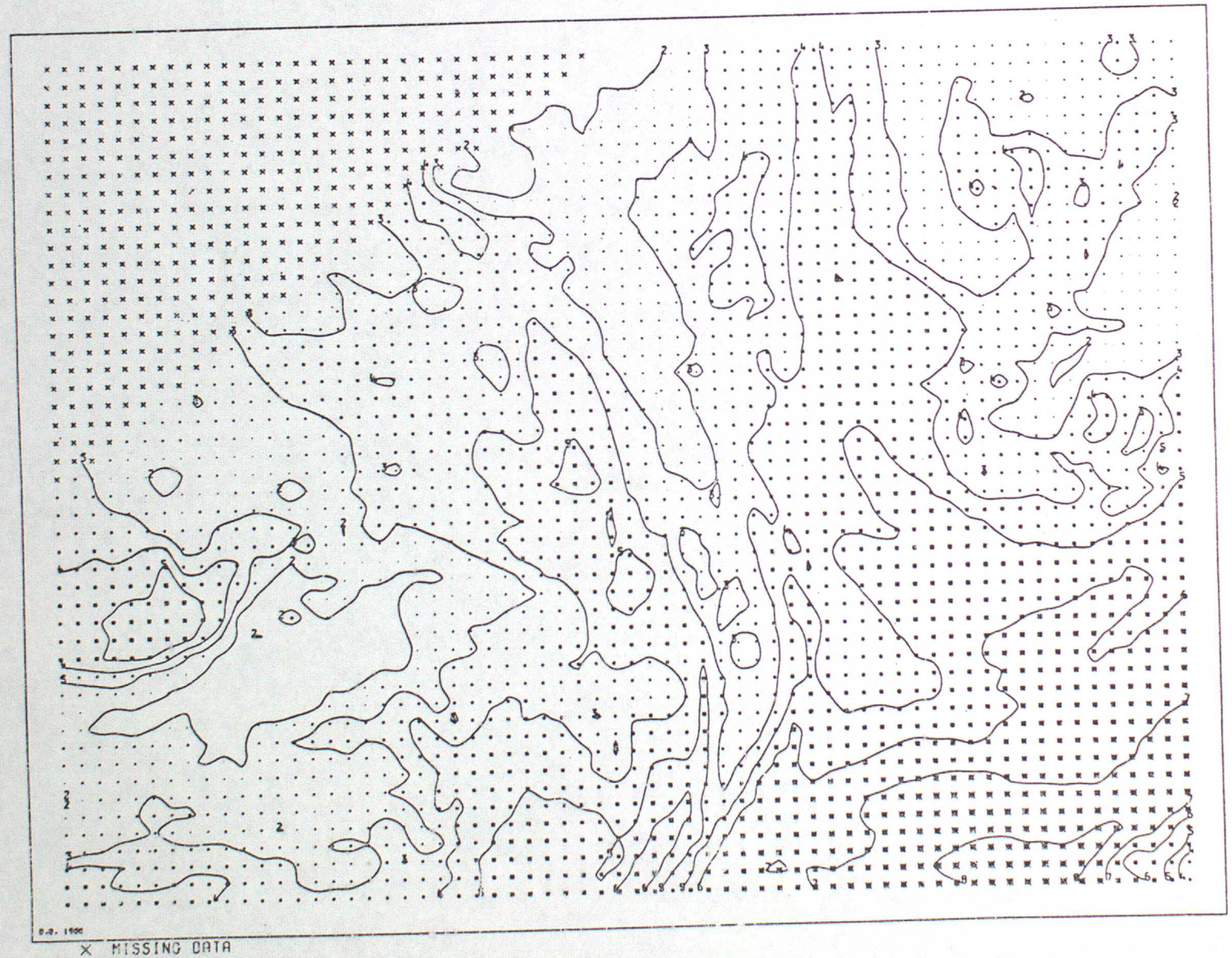

Units :
$mW\ m^{-2}\ sr^{-1}\ (cm^{-1})^{-1}$

Figure 3 Radiance field calculated with initial humidity field

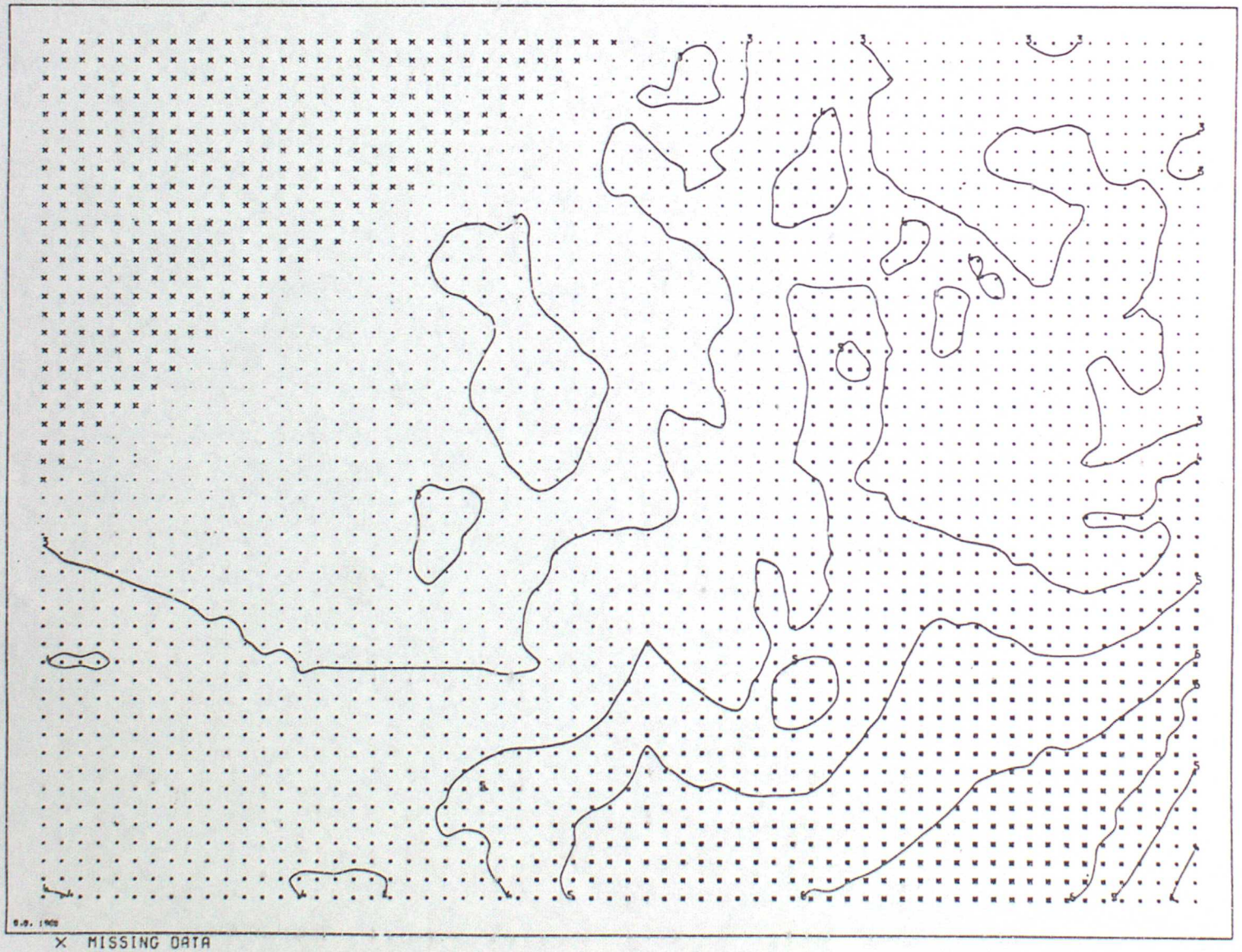

× MISSING DATA

Units :

mW m^{-2} sr^{-1} $(cm^{-1})^{-1}$

Figure 4 Absolute difference between measured radiances and radiances calculated with initial humidity field

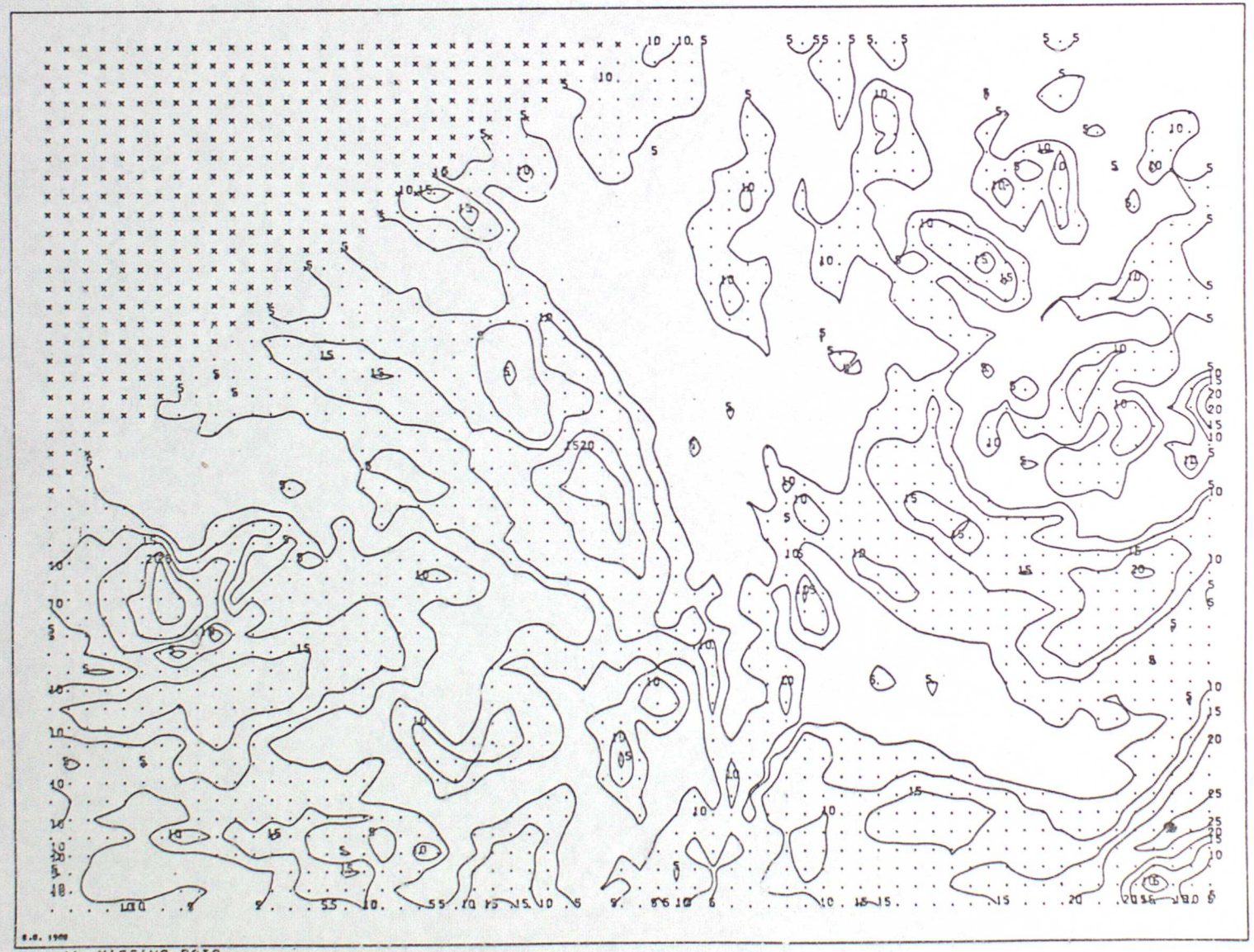

Units :

mW m^{-2} sr^{-1} $(cm^{-1})^{-1}$ x 10

Figure 5 Radiance field calculated with adjusted humidity field

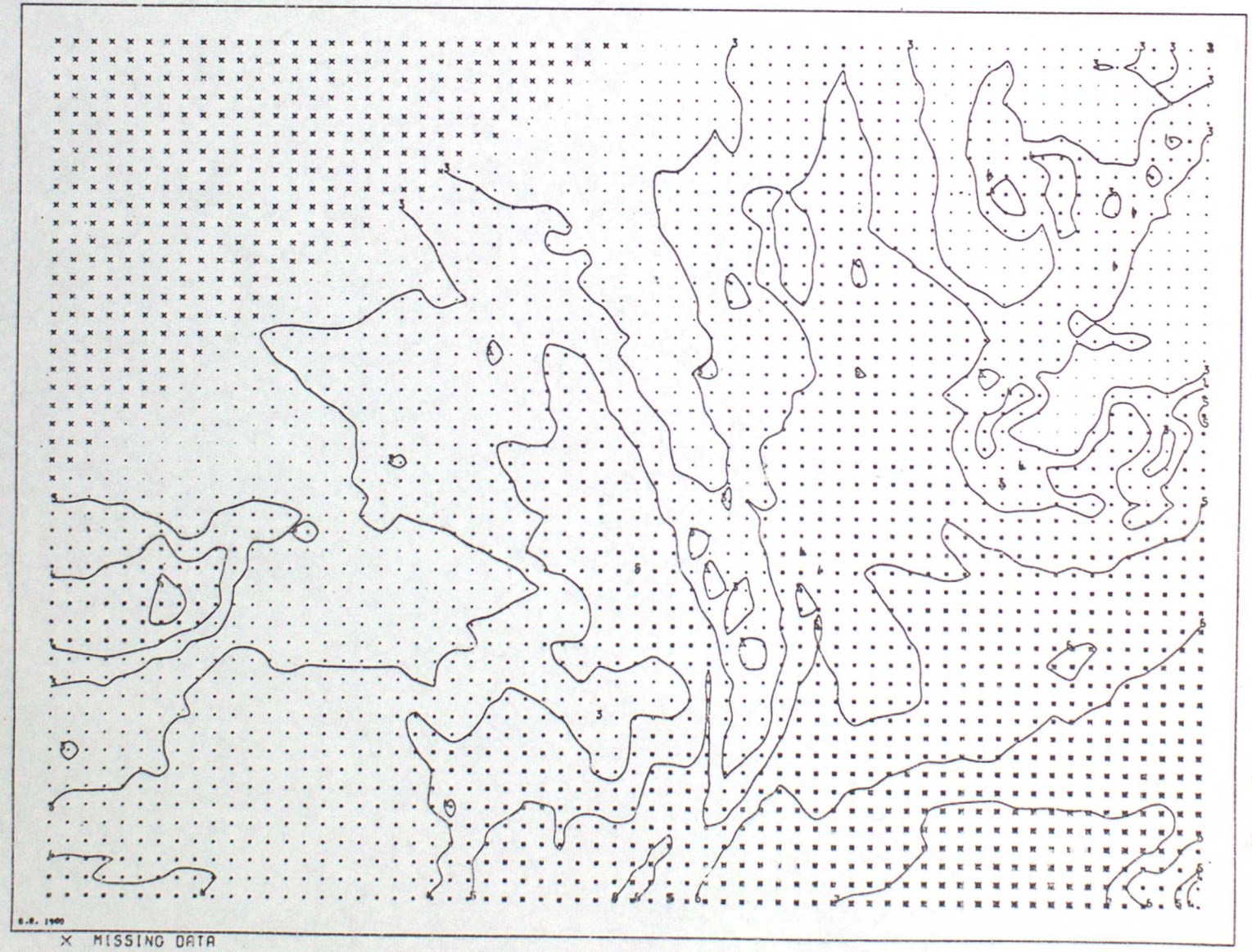

Units :

$mW\ m^{-2}\ sr^{-1}\ (cm^{-1})^{-1}$

Figure 6 Absolute difference between measured radiances and radiances calculated with adjusted humidity field

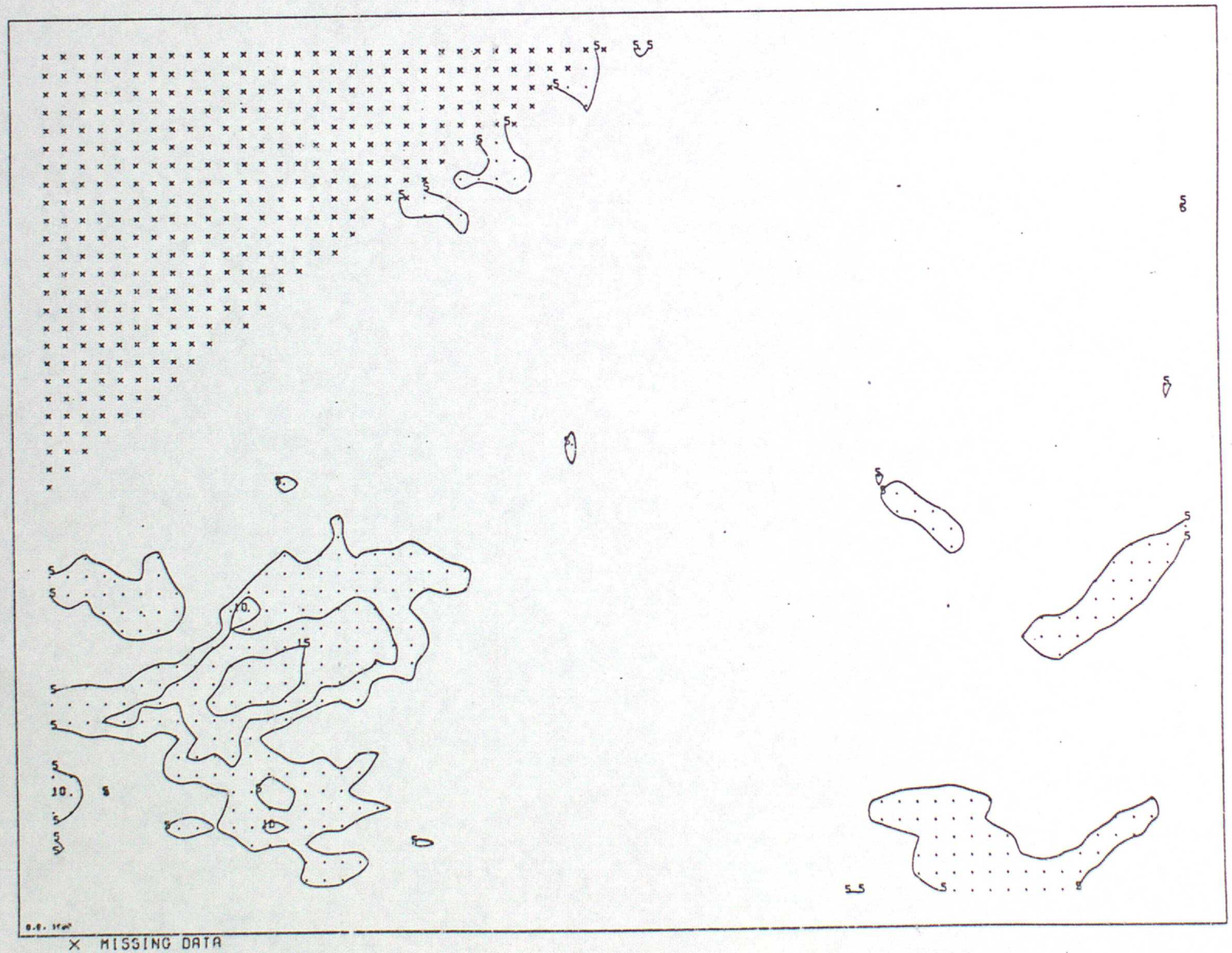

Units :

$mW\ m^{-2}\ sr^{-1}\ (cm^{-1})^{-1} \times 10$

Figure 7(a) Initial relative humidity field at 400 mb

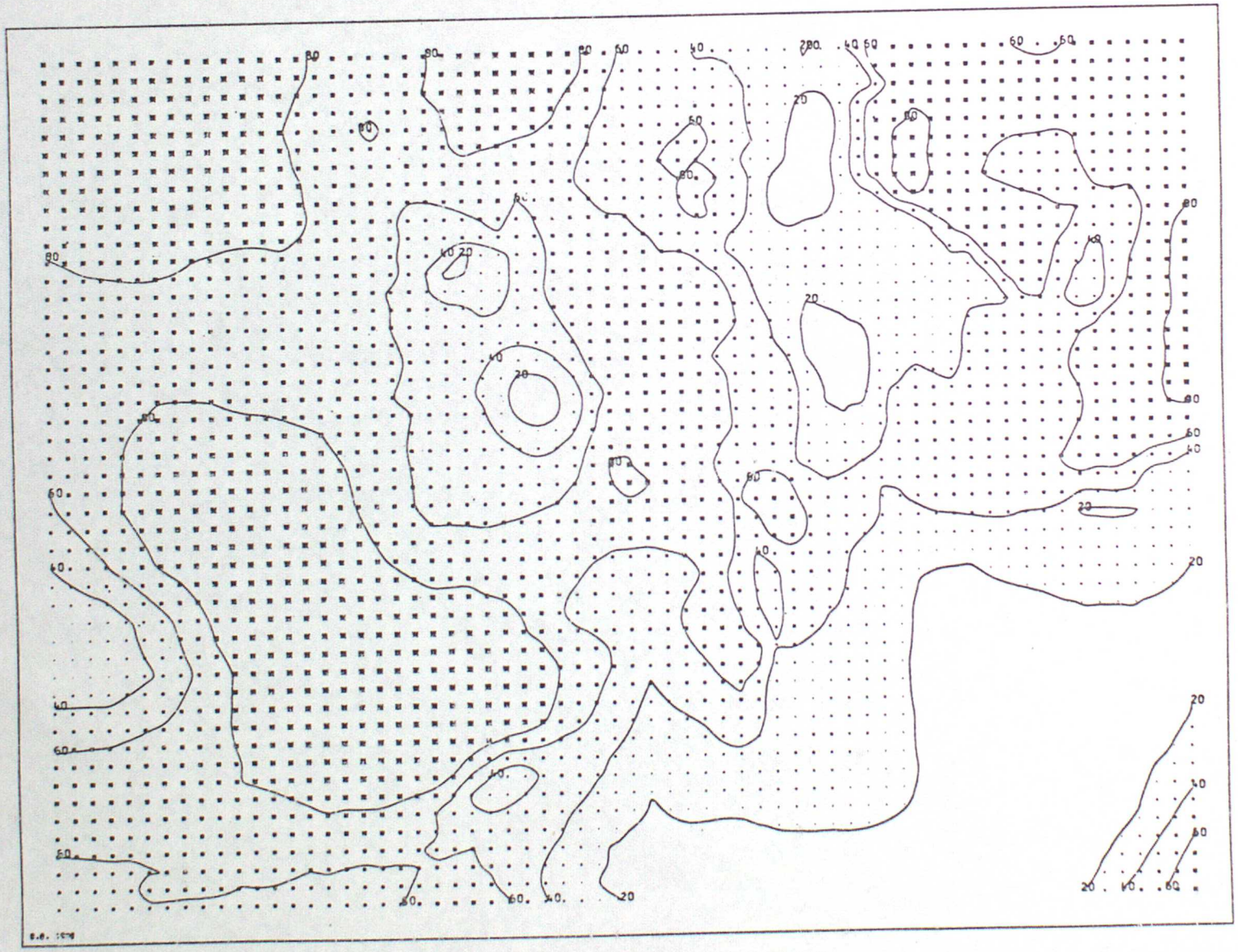

Units :

% relative humidity

Figure 7(b) Initial relative humidity field at 500 mb

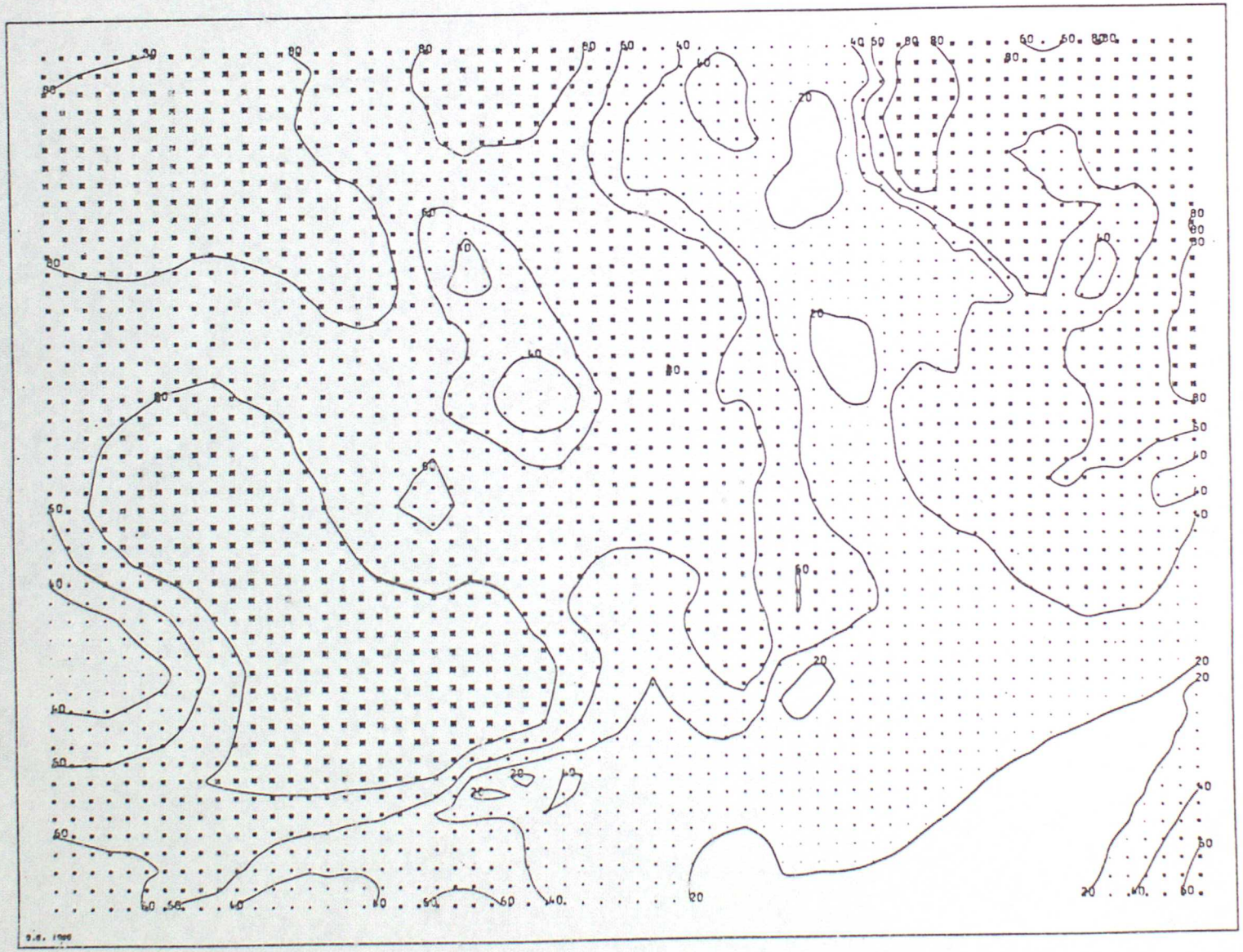

Units :

% relative humidity

Figure 8(a) Adjusted relative humidity field at 400 mb

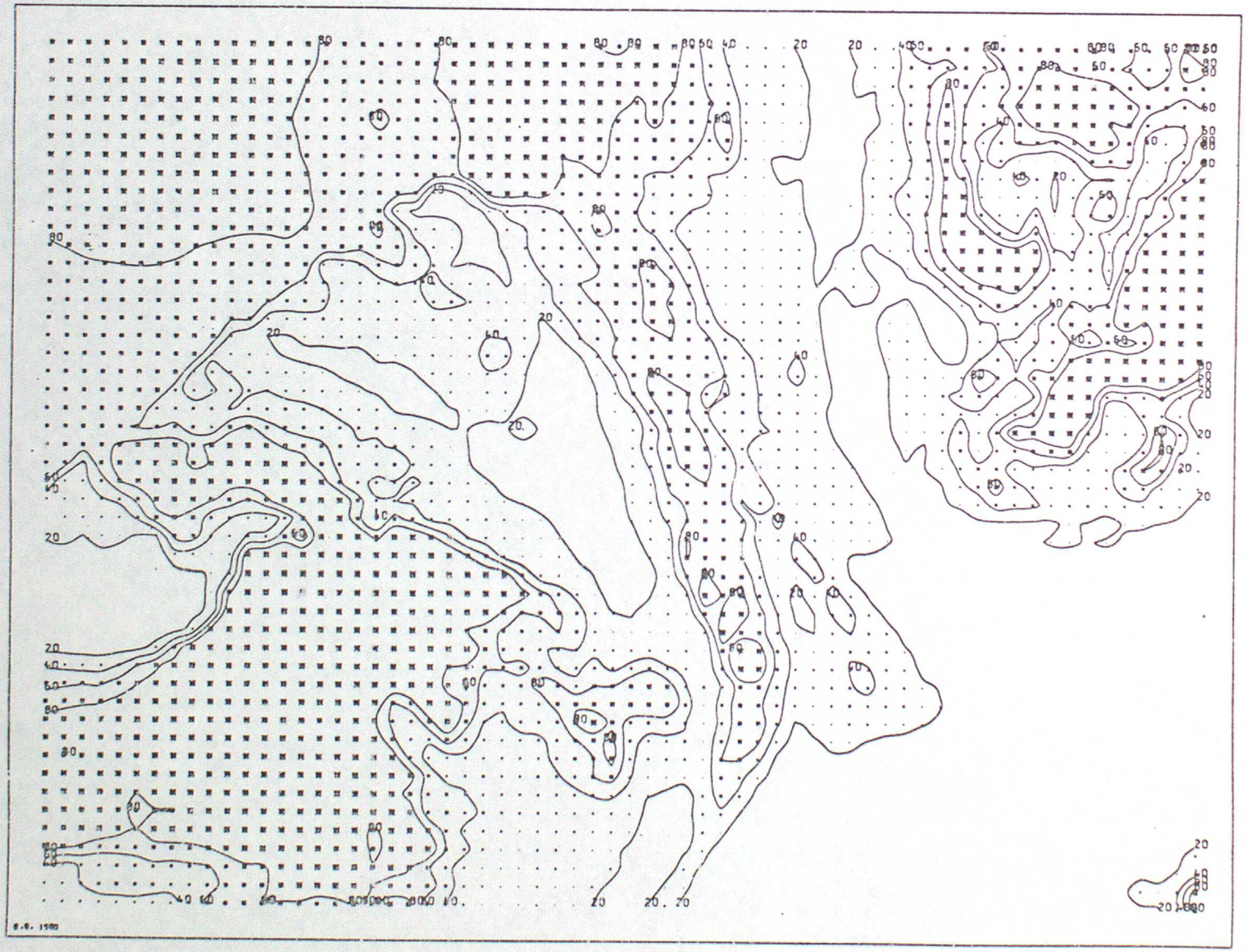

Units :

% relative humidity

Figure 8(b) Adjusted relative humidity field at 500 mb

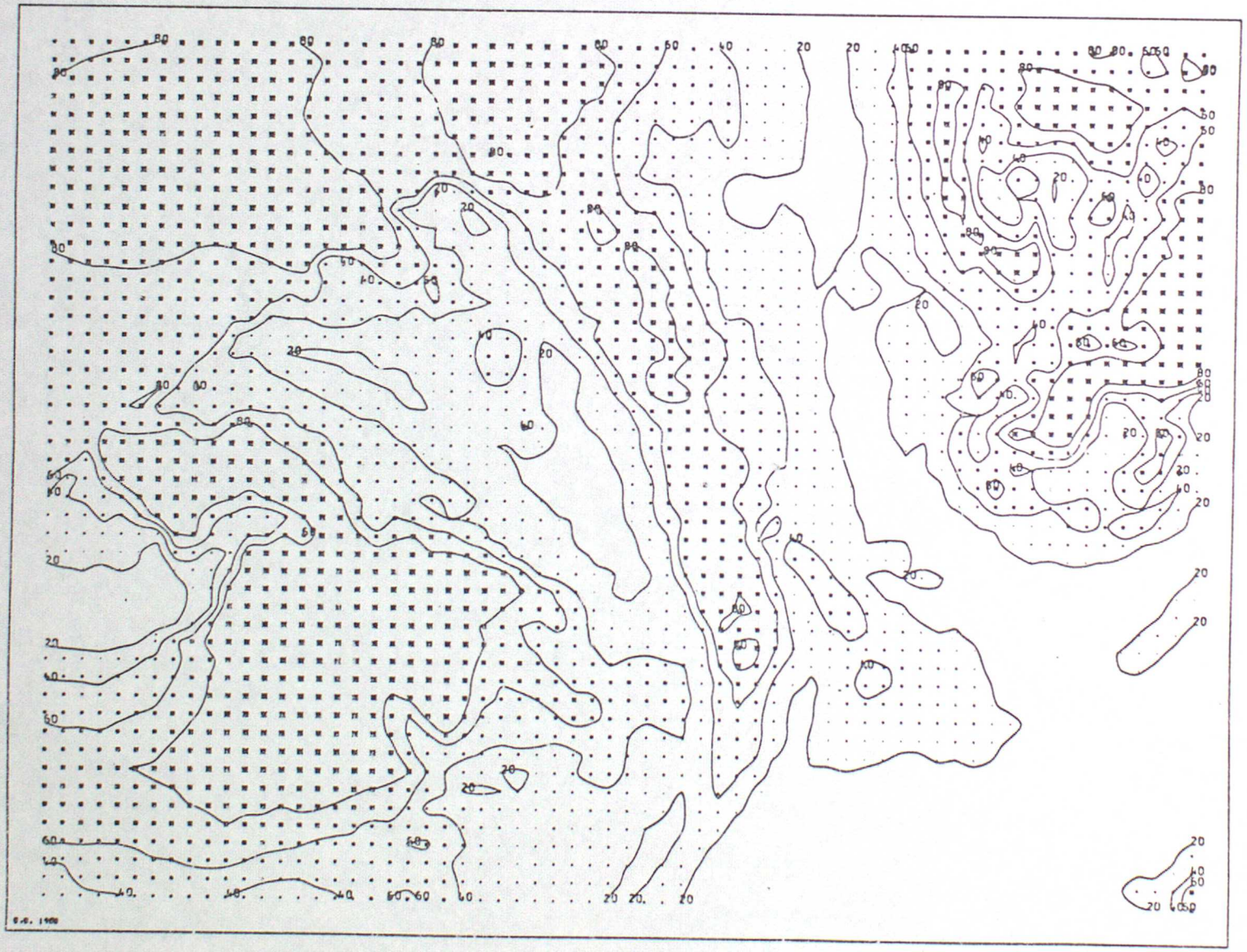

Units :

% relative humidity